RSC Advances

PAPER

View Article Online
View Journal | View Issue

Cite this: *RSC Adv.*, 2019, **9**, 34862

Synthesis of V-modified TiO_2 nanorod-aggregates by a facile microwave-assisted hydrothermal process and photocatalytic degradation towards PCP-Na under solar light

Rong Han,[ac] Jinwen Liu,*[b] Nan Chen,[ac] Gang Wang,[ac] Yakai Guo[ac] and Hongtao Wang[d]

Herein, novel V-modified titania nanorod-aggregates (VTNA), consisting of fine individual nanorods in radial direction, were fabricated *via* an efficient microwave-assisted hydrothermal (MWH) route. VTNA with high crystallinity and homogeneous mesopores were obtained by 30 min MWH processing at 190 °C; moreover, a mixed rutile–anatase phase appeared after vanadium doping. XPS analysis revealed that vanadium existed in the forms of V^{4+} and V^{5+} on the surface of MWV05 with V^{5+} being the dominant component, the content of which was approximately 3.5 times that of V^{4+}. Vanadium implanting was achieved efficiently by doping 0.5 and 1 at% V using a rapid MWH process and contributed towards the dramatic improvement of the visible-light response, with E_g decreasing from 2.91 to 2.71 and 2.57 eV with the increasing V doping content. MWV05 exhibited optimal photocatalytic degradation activity of water-soluble PCP-Na under solar light irradiation. The enhanced photodecomposition was attributed to the red-shift in the TiO_2 band-gap caused by vanadium impregnation, efficient charge separation due to the V^{4+}/V^{5+} synergistic effects and the free migration of charge carriers along the radial direction of the nanorods arranged in a self-assembled VTNA microstructure.

Received 8th August 2019
Accepted 7th October 2019

DOI: 10.1039/c9ra05480d

rsc.li/rsc-advances

1. Introduction

Among the advanced oxidation processes, the utilization of heterogeneous TiO_2 nanocatalysts is very promising in the field of environmental remediation, which has attracted significant attention of researchers working on non-biodegradable pollutant treatment, especially on the removal of hazardous organic pollutants.[1–7] Pentachlorophenol (PCP) and its salts, particularly sodium pentachlorophenate (PCP-Na), are highly chlorinated phenol derivatives listed as priority pollutants by the USA, European Union, and China.[8–10]

Heterogeneous photocatalysis has been conducted at room temperature under an open atmosphere utilizing natural solar light as the energy source; however, in heterogeneous photocatalysis, the catalysis of complex systems is performed mostly by employing pure TiO_2 nanoparticles under ultraviolet light (UV) irradiation due to the wide band gap (>3.0 eV) of TiO_2;[11–14] this indicates that only UV light can induce the catalysis, and hence, the practical application of TiO_2 under solar light is inefficient. Moreover, the high recombination rate of the photo-induced electron–hole pairs limits the efficiency of the photodecomposition of pollutants. Some efforts have been exerted to broaden the absorption region and enhance the photoactivity of TiO_2 by doping it with various transition metals ions.[15–19] Some V_2O_5/TiO_2 catalysts have shown optimal catalytic activities and good performances in the decomposition of chlorinated benzenes by vanadium impregnation on TiO_2.[5,7] Doping with vanadium appears to be one of the best alternatives to improve the solar photoactivity of a catalyst because of its synergetic effects on the extension of the absorption of TiO_2 in the visible light region and the separation efficiency of electron–hole pairs.[15,19,20]

The synthesis of semiconductors with various morphologies, such as nanorods or nanowires, and wider band gaps is receiving significant attention because of the potential applications of semiconductors in photocatalytic degradation.[21–25] Some investigations have found that well-crystallized TiO_2 nanorods exhibit high photocatalytic activity due to the free movement of carriers along the length of the one-dimensional nanostructure that can reduce electron–hole recombination.[23,25] Especially, the TiO_2 aggregates and TiO_2 aggregation behavior were investigated in aqueous matrices using natural

[a]*School of Environmental Science and Engineering, Chang'an University, Xi'an 710064, China*

[b]*School of Environmental and Municipal Engineering, Xi'an University of Architecture and Technology, Xi'an 710054, China. E-mail: 149983457@qq.com; Tel: +86-29-82339952*

[c]*Key Laboratory of Environmental Protection, Pollution and Remediation of Water and Soil of Shaanxi Province, Xi'an 710064, China*

[d]*School of Environment, Tsinghua University, Beijing 100084, China*

organic matter. The TiO_2 aggregates with high stability and appropriate hydrodynamic diameter in the complicated system could promote the capture and precipitation of TiO_2, thereby reducing its harm to the environment.[26,27]

Recently, the microwave-assisted hydrothermal method (MWH) has attracted significant interest in the preparation of nano-photocatalysts,[28–30] mainly in the form of nanoparticles. Compared with conventional heating, microwave-assisted preparation is characterized by a rapid heating rate, high energy efficiency, molecular homogeneity, selectivity, and convenience.[29–32]

Based on the abovementioned concepts, herein, the synthesis of nanocrystalline TiO_2 with distinct morphologies and vanadium modification through a novel MWH process from a commercially available raw material was conducted. The product was compared with the nanocatalysts fabricated *via* conventional hydrothermal treatment (HT). The textural properties, crystalline structures and chemical characteristics of the nanomaterials were examined by XRD, DRS, BET, and XPS. Batch experiments for the degradation of water-soluble PCP-Na were performed to evaluate the photocatalytic activity. This study presents an efficient synthesis of metal ion-doped TiO_2 photocatalysts, exhibiting high solar light photocatalytic ability and novel micro-structures, *via* a one-pot microwave-assisted hydrothermal method.

2. Experimental

2.1. Catalyst preparation

All chemicals used in this study were of analytical grade and used without further purification. Typically, 0.02 mol of $TiCl_4$ was added dropwise to 25 ml distilled water in an ice-water bath under vigorous magnetic stirring. After 4 h of stirring, a transparent solution was obtained, and 2 ml of hydrochloric acid (HCl, 36%) and a specific amount of NH_4VO_3 were dissolved in the abovementioned solution. For the MWH process, the resulting mixture was transferred to an 80 ml Teflon tube, sealed, and irradiated using a digestion microwave system (CEM, USA) at 150 and 190 °C for 30 min. For comparison, the traditional HT was also performed in an electric oven by heating at 190 °C for 20 h. The obtained precipitate was centrifuged and washed with deionized water and ethanol. Finally, the solid was dried at 80 °C for 24 h and ground in an agate mortar to obtain the final product.

The catalysts synthesized by MWH at 190 °C (or 150 °C) without and with V doping at the V/Ti molar ratios of 0.5% and 1% were denoted as MW0, MWV05, and MWV10 (MW0-150 and MWV10-150), respectively. The sample prepared by the conventional HT process at 190 °C was labeled as HT0.

2.2. Characterization of the photocatalyst

The crystalline phase of the samples was characterized by X-ray diffraction (XRD) using the Bruker D8 Advance Diffractometer with Cu Kα radiation ($\lambda = 1.5418$ Å), operated at 40 kV and 40 mA. The nitrogen adsorption–desorption isotherms and specific surface areas of the catalysts were measured using the Autosorb AS-1 N_2 adsorption apparatus (Quantachrome Instruments, USA) after vacuum degassing the samples at 150 °C. The UV-vis diffuse reflectance spectra (DRS) were characterized using the Hitachi U-3010 spectrophotometer equipped with an integrating sphere accessory for diffuse reflectance. The morphology of the samples was observed using the Hitachi S-5500 scanning electron microscope at the accelerating voltage of 20 kV. The surface composition of the nanocatalysts was analyzed by X-ray photoelectron spectroscopy (XPS) using the Kratos Axis Ultra System with monochromatic Al Kα X-rays (1486.6 eV).

2.3. Photocatalytic degradation

The photodecomposition of the PCP-Na solution was conducted to evaluate the photocatalytic activity of the prepared nanocatalyst under solar light. Photocatalytic degradation was performed in a strongly stirred batch reactor containing 250 ml of PCP-Na solution at various concentrations and 100 mg of the modified catalyst. Solar photocatalytic experiments were conducted using a cylindrical reactor covered with a quartz slice to maintain solar light spectrum, which was 34.2–19.7 mW cm^{-2}, as measured by a radiometer (FZ-A, China) in the afternoon of June from 2 : 30 pm to 4 : 30 pm at Beijing.

The starting pH value of the PCP-Na solution was approximately 6.4 ± 0.1. Solar illumination started after magnetically stirring the simulated PCP-Na suspension for 1 h in the dark.

2.4. Analytical determinations

To monitor the decomposition, 8 ml aliquots were drawn at regular intervals from the vigorously stirred solution. The mixture was filtered directly through a 0.45 μm membrane filter. PCP-Na in the filtrates was determined by an HPLC system (Shimadzu model LC-10AVP) equipped with a YMC C-18 reverse phase column (25 μm × 4.6 mm × 250 mm) and a UV detector at 249 nm for PCP-Na. The mobile phase was 80% methanol in pH 2 phosphate buffer with the flow rate of 1.0 ml min^{-1}. The UV spectra of the aqueous solution were obtained by a UV-vis spectroscope (UV-2401PC, Shimadzu).

3. Results and discussion

3.1. XRD patterns of the photocatalysts

Fig. 1 illustrates the XRD patterns of the catalysts prepared at different reaction temperatures (150 and 190 °C) by microwave-assisted synthesis with and without V doping and the sample fabricated by conventional HT at 190 °C. An increase in the MWH temperature from 150 to 190 °C resulted in narrower and sharper diffraction peaks, which indicated high degree of crystallization when the microwave temperature was increased to 190 °C after 30 min irradiation.

The products obtained from MWH and HT processing without V doping showed a single rutile phase of titania according to the diffraction peaks, consistent with those of TiO_2 in the rutile form (JCPDS 21-1276). However, a mixed phase consisting of the anatase and rutile phases was detected in the V-doped nanocatalyst obtained by the MWH synthesis. Tiny

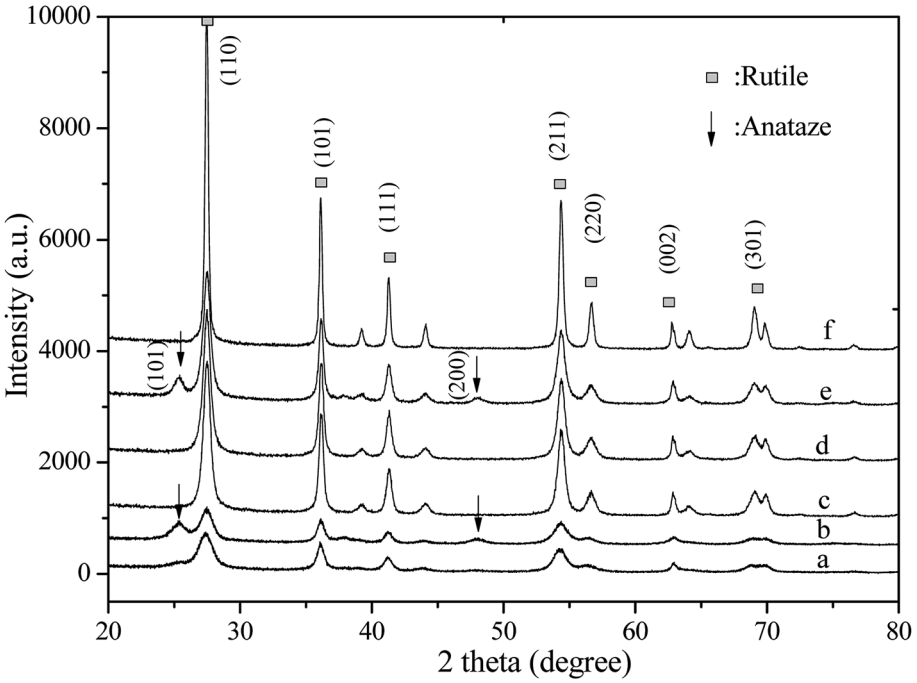

Fig. 1 XRD patterns of the (a) MW0-150, (b) MWV10-150, (c) MW0, (d) MWV05, (e) MWV10, and (f) HT0 nanocatalysts.

peaks around 25.3° and 48.0°, corresponding to the anatase (101) and (200) crystal planes (JCPDS 21-1272), appeared, indicating that V doping induced the transformation of TiO_2 from the rutile phase to the anatase phase; moreover, a mixed phase consisting of the anatase and rutile phases was obviously detected in MWV10 with 1 at% V doping. The diffraction peak intensity of the rutile phase changed slightly under MWH at 190 °C by V doping (Table 1).

The rutile phase is usually the thermally stable phase. The transformation from the anatase to the rutile phase has been previously reported.[33] The anatase component can be dissolved in concentrated HCl and recrystallized to the rutile phase *via* dissolution-crystallization.[34] Some investigations have indicated that the mixed anatase and rutile phases result in high activity of TiO_2, which is ascribed to the effective separation of photo-generated electron and hole pairs by the presence of interface junction and oxygen vacancy at the phase interface.[35,36] Therefore, the modified catalyst, which consisted of an anatase and a rutile phase mixture, synthesized in the present method was also anticipated to possess high photocatalytic activity.[37]

Furthermore, the MWT treatment provided an efficient route to obtain TiO_2 crystallites. The synthesis time is as short as 30 min, which is unattainable for a reaction *via* conventional HT.[32,34] Good TiO_2 crystallites and remarkably effective heating together with low energy consumption were achieved *via* the preparation of modified catalysts by the efficient microwave irradiation method.

The intensity of the diffraction peaks for HT0 was significantly stronger than that for the sample synthesized by the MWH method due to the requirement of long reaction time at 190 °C. The diameter of the narrow part of the nanocatalyst was 31.1–42.8 nm and 13.7–24.0 nm for the catalyst fabricated by HT and MWH (Table 1), respectively, calculated from the various angles, namely, 27.5, 36.2, 41.2, 54.3, and 56.6°, in the XRD patterns of the rutile phase.[38] A smaller microstructure was exhibited by the catalyst synthesized by the MWH method.

Table 1 Physicochemical properties of the nanocatalysts synthesized by the HT and MWH methods

Sample	Crystalline size[a] (nm)	Intensity$_{(110)}$[b]	Surface area[c] ($m^2\ g^{-1}$)	Pore volume[d] ($cm^3\ g^{-1}$)	Pore diameter[e] (nm)
HT0	31.1–42.8	5844	10.35	0.039	3.348
MW0	13.7–24.0	2823	17.89	0.029	3.852
MWV05	13.0–23.6	2734	12.57	0.022	3.784

[a] Average crystalline size determined by XRD using the Scherrer equation and the rutile diffraction peaks. [b] Intensity$_{(110)}$ is the height intensity of the (110) rutile diffraction peak at 27.5°. [c] Specific surface area data calculated from multi-point Brunauer–Emmett–Teller method. [d] Pore volume obtained from the nitrogen adsorption volume at P/P_0 of 0.994. [e] Pore diameter estimated from the desorption isotherm by the BJH model.

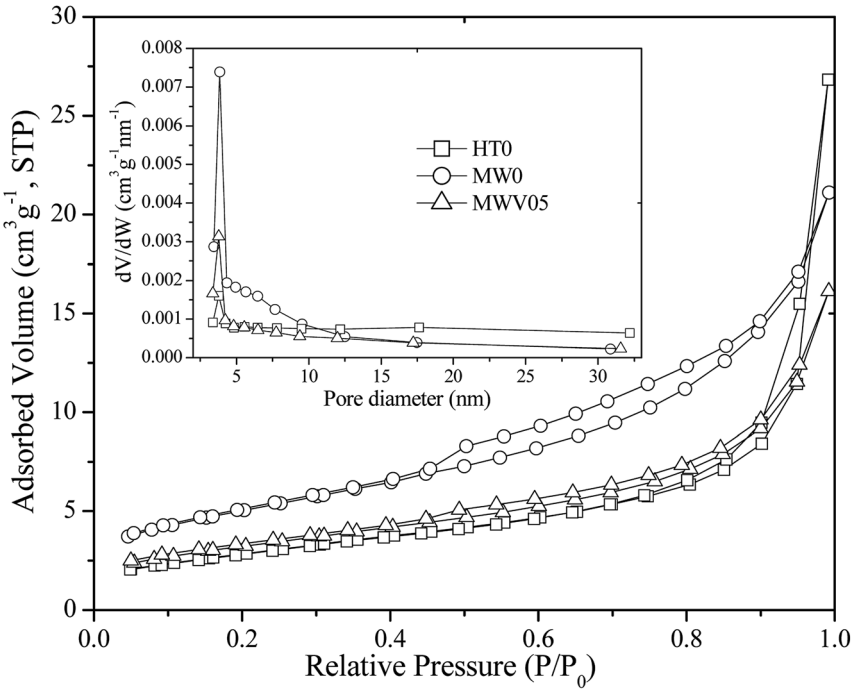

Fig. 2 Nitrogen adsorption–desorption isotherm and pore size distribution curve (inset) of the synthesized nanocatalysts.

3.2. BET surface areas and pore distributions

The microstructures of the synthesized catalysts were determined by nitrogen adsorption–desorption (Fig. 2). The adsorption isotherm of MW0 and MWV05 is typically of type IV, which confirms a homogeneous distribution of uniform mesopores within the nanomaterials. The type H1 hysteresis loop of MW0 is representative of the presence of tubular or bottle-neck shaped pores. MWV05 is characterized by a type H3 hysteresis loop, which is characteristic for aggregates with a non-defined mesoporosity or pores with an interconnected lamellar structure.[39] The HT0 curve corresponds to a type II isotherm and type H4 hysteresis loop, mainly indicating narrow slit-shaped pores or macropores.[40]

Compared with the case of the porous structure of HT0 (Table 1), the pore volume decreased and the average pore diameter increased in the samples fabricated by the MWH method. The calculated pore size distribution curves (inset, Fig. 2) from the desorption branch of the nitrogen isotherm suggested that the BJH distribution of HT0, MW0, and MWV05 had similar peaks at approximately 3.75, 3.85, and 3.78 nm, respectively, whereas MW0 and MWV05 had a more concentrated pore size distribution and uniform pore channels of the mesoporous structure when compared with HT0. The Brunauer–Emmett–Teller (BET)-specific surface area of MW0 was larger than that of HT0, whereas it decreased with an increase in the V doping content.

3.3. Morphology and structure

Fig. 3 shows the SEM images of the HT0, MW0, and MWV05 nanocatalysts. As observed from Fig. 3A, HT0 has a nanorod structure. The length of HT0 was about 100–300 nm, and its width was about 30–50 nm, consistent with the values calculated from XRD.

The morphology of the catalysts synthesized by the MWH process exhibited a three-dimensional nanorod-aggregate microstructure, which had the diameter of 1–2 μm and was composed of numerous individual nanorods radiating from the center to the rim of the microstructure (Fig. 3B and C). This morphology of VTNA appears very much like a chrysanthemum, and the internal nanorods were similar to the petals of a flower. The nanorod in the VTNA is evidently smaller than that in the catalyst synthesized by HT, with a diameter of approximately 15–30 nm and length of approximately 100–200 nm. The space among the nanorods is arranged along the radial direction. The morphology of the MWH products was slightly influenced by V doping. In other words, the structure and feature of VTNA were not destroyed after the introduction of vanadium during the microwave-assisted hydrothermal treatment. Li also found that a sample doped with V ions had morphology consistent with that of neat TiO_2.[40]

The synthesis mechanism of the VTNA *via* the MWH method is considered as follows: under microwave irradiation, many small nanoparticles initially precipitate to form a core. After this, the particles aggregate with each other *in situ* and self-assemble into large nanorods in the radial direction. The irradiation features of microwave processing, accelerated reaction, and *in situ* diffusion from the inside of the aqueous precursor media play crucial roles in the formation of this morphology;[41] compared with the case of the MWH process, the strong convection heat transfer in the traditional HT method results in irregularly arranged large nanorods.[32]

3.4. UV-vis DRS

Fig. 4 shows the DRS of the catalyst prepared by the MWH and HT methods at 190 °C. The samples prepared without the V

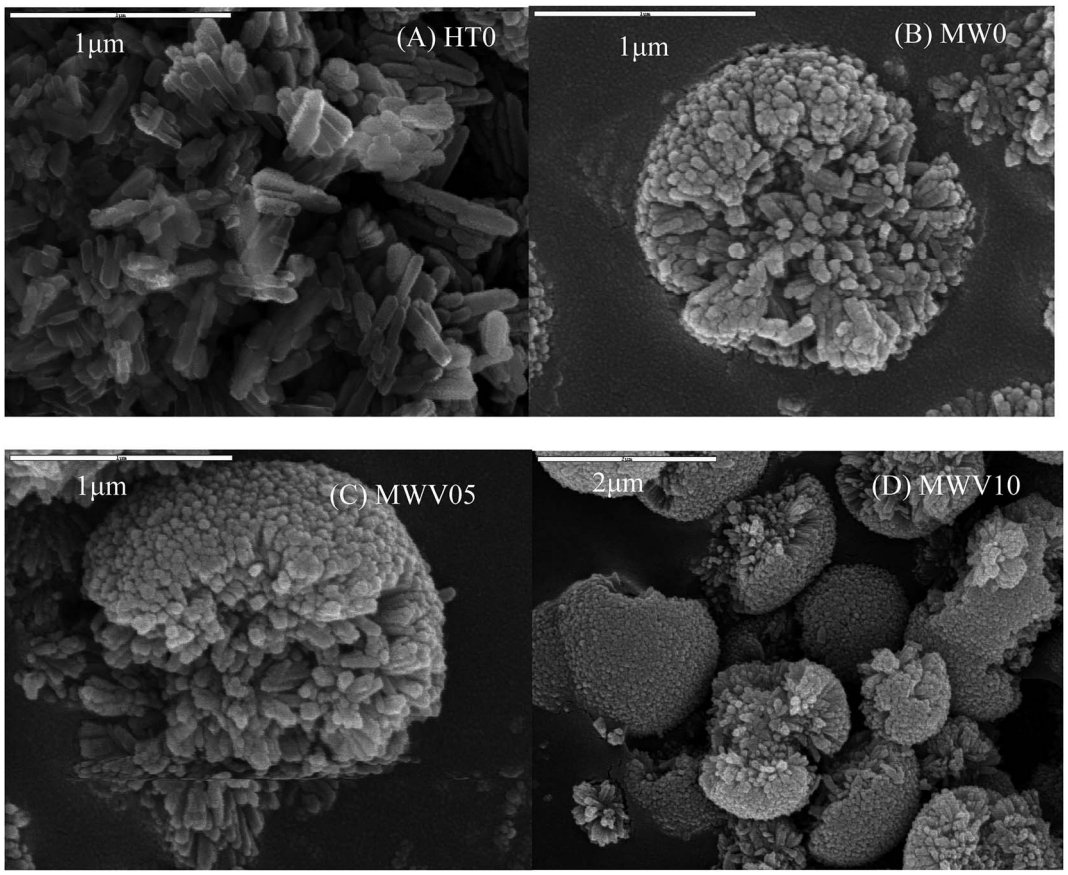

Fig. 3 SEM images of the prepared (A) HT0, (B) MW0, (C) MWV05, and (D) MWV10 nanocatalysts.

dopant, HT0 and MW0, presented only UV light (<400 nm) absorption. Notable visible-light absorption in the range of 400–700 nm, as displayed in MWV05 and MWV10 with V-doping under MWH processing. The visible-light absorption capacity of the catalyst increased with an increase in the V doping amount in the starting solution. The band-gap energies (E_g) were obtained by the Kubelka–Munk equation (Fig. 4). The theory of interband optical absorption indicates that the absorption coefficient of a semiconductor can be expressed as[42]

$$[F(R)h\nu]^{1/2} = A(h\nu - E_g) \quad (1)$$

where $F(R)$ represents the experimental absorption coefficient data of DRS, A is a constant, $h\nu$ is calculated from the equation $h\nu = 1240/\lambda$, and 1/2 is a value characterizing the transition process for indirect TiO_2. Therefore, the band gap value can be determined by extrapolating the decreasing portion of the spectrum to the abscissa at zero absorption.[42,43] Herein, E_g decreased from 2.91 to 2.71 and to 2.57 eV for MW0, MWV05, and MWV10, respectively, which was attributed to the formation of an impurity energy state within the titanium band-gap;[19] this demonstrated that effective V implanting could be achieved through the fast MWH process.

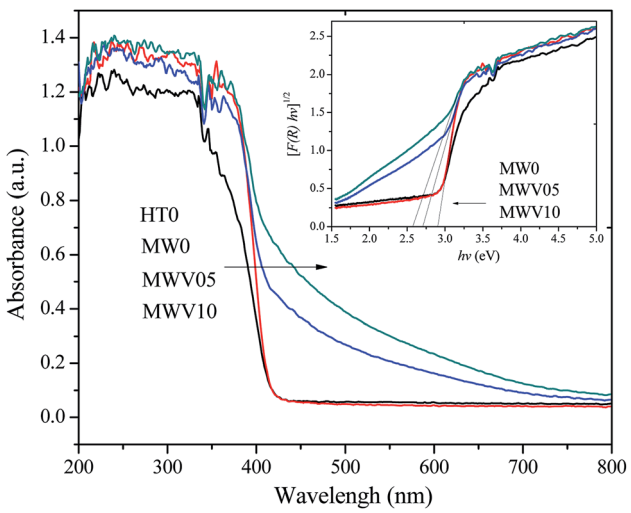

Fig. 4 The UV-vis DRS and the corresponding band energy (inset) of the synthesized TiO_2 samples.

3.5. XPS analysis

The atomic compositions and chemical characteristics of the surface elements in the modified TiO_2 were investigated by the XPS analysis. The chemical states of the Ti 2p, O 1s, and V 2p

species of MWH05 were obtained by analyzing the XPS core levels (Fig. 5A–C).

As shown in Fig. 5A, the double peaks in the Ti 2p region are assigned to the spin–orbit coupling of Ti $2p_{3/2}$ and Ti $2p_{1/2}$. The Ti^{4+} $2p_{3/2}$ and Ti^{4+} $2p_{1/2}$ peaks for MWV05 could be fitted at 458.7 and 464.4 eV, separated by 5.7 eV, and the area ratio of the two peaks was approximately 1.95, which were in accordance with those of Ti^{4+}.[44,45] The corresponding peaks of Ti^{3+} $2p_{3/2}$ and Ti^{3+} $2p_{1/2}$ cannot be fitted and found for the titania lattice. Therefore, Ti existing in the form of Ti^{4+} without a low valence, such as Ti^{3+}, may be ascribed to the low content of the dopant[46] and oxidation by the abundant adsorbed water and hydroxyl groups[47] during the microwave-assisted hydrothermal synthesis process.

It appears from Fig. 5B that O 1s in the high-resolution XPS spectrum of MWV05 can be fitted into three peaks centered at 529.9, 530.8, and 532.1 eV. The fitting peaks were ascribed to crystal lattice oxygen, hydroxyl group oxygen, and surface contaminant oxygen on the surface of the doped TiO_2,[48] which accounted for 79.4%, 12.9%, and 7.7% relative atomic percentages of O in MWV05, respectively.

The XPS spectrum of the V 2p region for MWV05 is shown in Fig. 5C. The spectrum corresponding to V $2p_{3/2}$ of the VTNA sample can be divided into two peaks centered at 515.9 and 517.1 eV, which are assigned to V^{5+} $2p_{3/2}$ and V^{4+} $2p_{3/2}$ incorporated into the crystal lattice of MWV05, respectively.[40,48] The fitting data demonstrate that V^{5+} is the dominant component on the surface of the doped TiO_2, the content of which is approximately 3.5 times that of V^{4+}, as indicated by the area under the V $2p_{3/2}$ peak. The V precursor (NH_4VO_3) was the source of V^{5+}, whereas the V^{4+} species might have been formed during the synthesis by the reduction of the V^{5+} species. Since the ionic radii of the V^{4+} (0.058 nm) ion is close to that of Ti^{4+} (0.064 nm), the V^{4+} ions can be easily incorporated into the TiO_2 lattice by replacing the Ti^{4+} ions *via* substitution, and the Ti–O–V bond is formed.[1,15,45] The substitution of the Ti^{4+} ions by the V^{5+} ions may cause the delocalization of the valence electron around the V^{5+} positive center and thus results in the formation

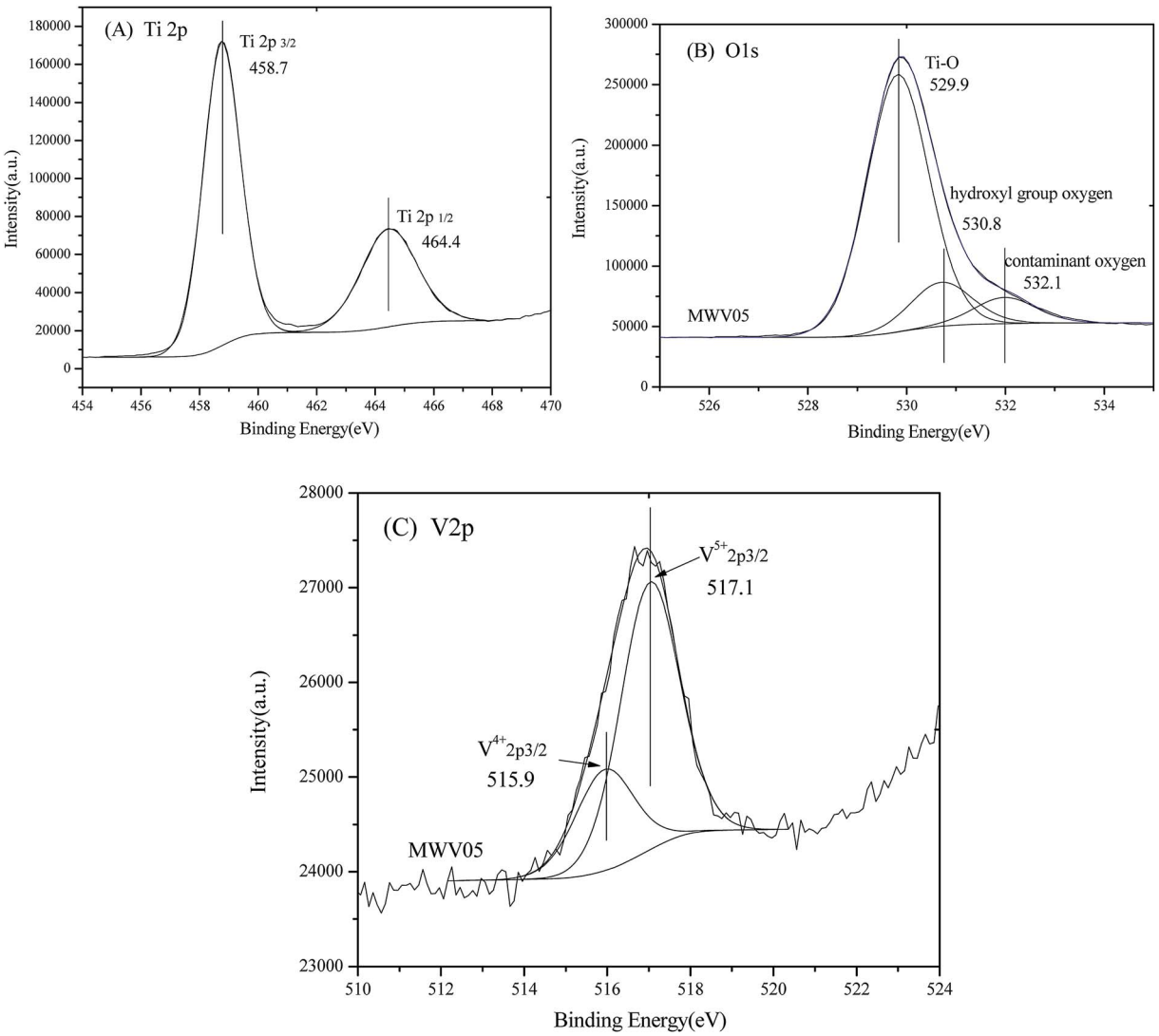

Fig. 5 High-resolution XPS spectra and chemical states fitting of the (A) Ti 2p region; (B) O 1s region; and (C) V 2p region of MWV05.

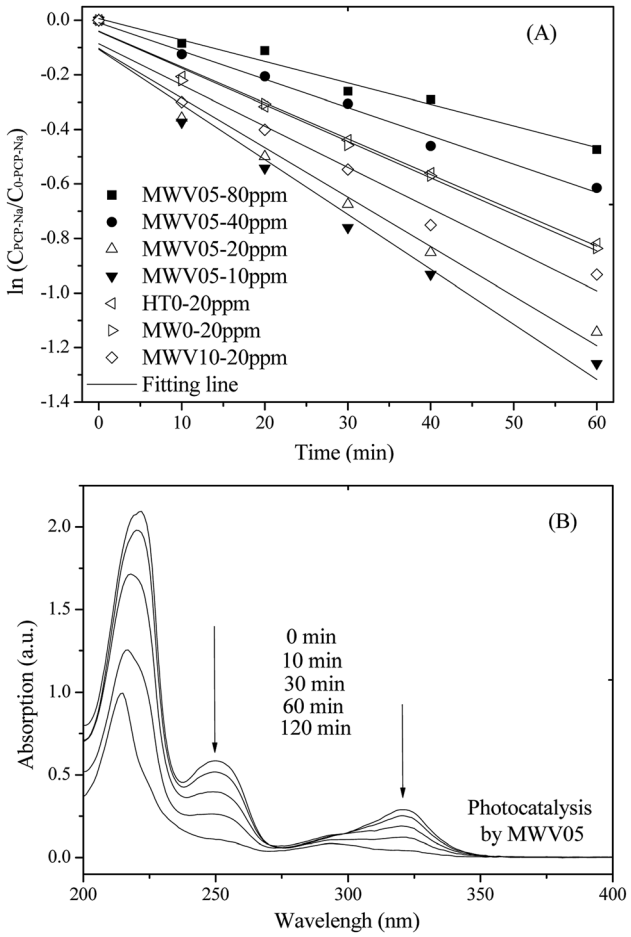

Fig. 6 The first-order reaction kinetics of PCP-Na (10–80 ppm) degradation (A) and UV spectral changes of PCP-Na (20 ppm) by MWV05 (B) as a function of irradiation time.

of a localized surface charge on the sample.[48] Vanadium species with a mixed-valence consisting of V^{4+} and V^{5+} has the tendency to be on the lattice surface and may form shallow potential wells, improving the separation efficiency of photo-generated charges.[48]

3.6. Photodegradation of PCP-Na under solar light

The degradation process of PCP-Na (20 ppm) over the synthesized catalysts was investigated to define the photocatalytic activity of the catalysts. The process could be described by the apparent first-order kinetics model according to the equation $-\ln(C/C_0) = kt$. Fig. 6A shows the linear relationship between $\ln(C_{\text{PCP-Na}}/C_{0\text{-PCP-Na}})$ and irradiation time during the PCP-Na photodecomposition; the apparent reaction rate constants ($k_{\text{PCP-Na}}$) are listed in Table 2. The photocatalytic activity of MW0 was similar to that of the HT0 nanorods under solar light. The photocatalytic activity of MWV05 was higher than that of MW0 mainly due to the strong visible light absorption and efficient electron–hole separation in the former case; this demonstrated that V doping was beneficial for the enhancement of photoactivity by the developed MWH technology with a very short processing time of 30 min. The anatase–rutile mixed phase of MWV10, with more anatase phase and interface junction than those in MWV05, is anticipated to benefit the photocatalytic interface reaction. However, the activity of MWV10 evidently decreased with the increasing V implantation *via* the MWH treatment; this indicated that an appropriate amount of V ions was necessary, and slightly overloaded V doping resulted in the easier recombination of the generated electron–hole pairs. When the doping ratio is more than 0.5 at%, large amount of electrons may be trapped by the V 2p levels and consumed by the V^{4+}/V^{5+}sites, instead of participating in the photocatalytic degradation.[1,48]

The UV spectral variations during the PCP-Na photodegradation using MWV05 are illustrated in Fig. 6B. The PCP-Na aqueous solution exhibited two major absorption peaks at 249 and 320 nm, which were attributed to the conjugated structure.[49] The absorption intensities at 249 and 320 nm decreased with the solar light-induced photocatalysis. The influence of the initial PCP-Na concentration on the rate of the photocatalytic reaction conducting utilizing MWV05 was also determined. The degradation rate increased when the initial concentration of PCP-Na decreased. Therefore, the initial PCP-Na concentration is critical to the rate of photodegradation over the VTNA catalyst.

Optimally low ratio of vanadium in the modified VNTA was mainly responsible for the efficient separation of electron–hole pairs by the interaction of V^{4+} and V^{5+}. The V^{5+} species act as electron trapping center.[48] The V^{4+} species was easily detrapped, and the electrons were transferred to the oxygen molecules adsorbed on the surface of titanium to produce the oxidant superoxide radical ion O_2^-.[45,48] Moreover, well-crystallized TiO_2 nanorods in the nanorod-aggregates may exhibit high photocatalytic activity due to the free movement of carriers along the length of nanorod and along the radial direction of the nanorods arranged in VTNA. The free movement of carriers in the VTNA nanostructure can reduce electron–hole recombination. Moreover, abundant holes are transferred to the surface to take part in the photoreactions, and the produced hole and O_2^- can react with H_2O and H^+ to produce hydroxyl radical according to the following reactions:

Table 2 Apparent first-order rate constant $k_{\text{PCP-Na}}$ (min^{-1}) of the initial reactions for the photocatalytic degradation of PCP-Na under solar light irradiation

Catalyst	MWV05				HT0	MW0	MWV10
$C_{0\text{-PCP-Na}}$	80 ppm	40 ppm	20 ppm	10 ppm	20 ppm	20 ppm	20 ppm
$k_{\text{PCP-Na}}$	0.0079	0.0104	0.0182	0.0202	0.0132	0.0134	0.0151
R^2	0.9741	0.989	0.967	0.971	0.990	0.988	0.957

$$\text{Modified VTNA} \xrightarrow{\text{solar radiation}} h + e^{-}(\text{solar light excitation}) \quad (2)$$

$$V^{5+} + e^{-} \rightarrow V^{4+}, \rightarrow V^{4+} + O_2\,(\text{surface}) \rightarrow V^{5+} + \cdot O_2^{-}$$
(e^{-} separation and transfer along the nanorod) (3)

$$3\cdot O_2^{-} + 4H^{+} \rightarrow 2\cdot OH + 2\cdot OOH \quad (4)$$

$$h + H_2O\,(\text{surface}) \rightarrow \cdot OH + H^{+}$$
(production of oxidative species) (5)

$$PCP^{-} + \cdot OH/\cdot O_2^{-} \rightarrow \text{decomposition} \quad (6)$$

4. Conclusions

This study reports a novel MWH process for the preparation of V-modified three-dimensional titania nanorod-aggregates, which can be captured and recycled easily; the morphology characterized as a chrysanthemum composed of small individual nanorods in the radial direction has been achieved by the rapid MWH process. The irradiation features of the MWH processing, accelerated reaction, and *in situ* diffusion from the inner part of aqueous precursor media were responsible for the formation of the fine VTNA microstructure. A highly crystallized single rutile phase was achieved without V doping at 190 °C, and a mixed phase consisting of anatase and rutile appeared in the VTNA samples with V implanting. The doped VTNA had a homogeneous distribution of uniform mesopores, confirmed by the nitrogen adsorption isotherm. Notable improvement in the visible-light absorption capacity, with E_g decreasing from 2.91 to 2.71 and 2.57 eV, was achieved by 0.5 at% and 1 at% V doping utilizing the efficient MWH process. XPS analysis reveals that vanadium exists in the form of V^{4+} and V^{5+} on the surface of VTNA. V^{5+} was the dominant component on the surface of MWV05, the content of which was approximately 3.5 times that of V^{4+}. Furthermore, MWV05 with 0.5 at% V doping exhibited optimal photocatalytic degradation activity of water-soluble PCP-Na under solar light irradiation. The enhanced photodecomposition has been attributed to the efficient red-shift in the band-gap of the TiO_2 lattice by vanadium incorporation, efficient charge separation due to V^{4+}/V^{5+} synergistic effects and the free migration of charge carriers along the radial direction of the nanorods arranged in VTNA. This study may provide a new insight into the fast synthesis of ion-implanted nanomaterials with self-assembled morphological features by efficient microwave-assisted approaches.

Conflicts of interest

There are no conflicts to declare.

Acknowledgements

The authors appreciate the generous financial support received from the National Natural Science Foundation of China (No. 21407012), the Natural Science Basic Research Plan in Shaanxi Province of China (No. 2015JQ5178), the Fundamental Research Funds for the Central Universities (No. 300102298201), the Opening Foundation of Shaanxi Key Laboratory of Exploration And Comprehensive Utilization of Mineral Resources (No. 2014HB005), and the Special Fund for Basic Scientific Research of Central Colleges, Chang'an University (310829163406).

References

1 J. Nesic, D. D. Manojlovic, I. Andelkovic and B. P. Dojcinovic, Preparation, characterization and photocatalytic activity of lanthanum and vanadium co-doped mesoporous TiO_2 for azo-dye degradation, *J. Mol. Catal. A: Chem.*, 2013, **378**, 67–75.

2 K. Dai, T. Y. Peng, H. Chen, J. Liu and L. Zan, Photocatalytic degradation of commercial phoxim over La-doped TiO_2 nanoparticles in aqueous suspension, *Environ. Sci. Technol.*, 2009, **43**, 1540–1545.

3 C. Lettmann, K. Hildenbrand, H. Kisch, W. Macyk and W. F. Maier, Visible light photodegradation of 4-chlorophenol with a coke-containing titanium dioxide photocatalyst, *Appl. Catal., B*, 2001, **32**, 215–227.

4 K. Dai, T. Y. Peng, H. Chen, R. X. Zhang and Y. X. Zhang, Photocatalytic degradation and mineralization of commercial methamidophos in aqueous titania suspension, *Environ. Sci. Technol.*, 2008, **42**, 1505–1510.

5 J. Wang, X. Wang, X. L. Liu, T. Y. Zhu, Y. Y. Guo and H. Qi, Catalytic oxidation of chlorinated benzenes over V_2O_5/TiO_2 catalysts: The effects of chlorine substituents, *Catal. Today*, 2015, **241**, 92–99.

6 C. Gannoun, A. Turki, H. Kochkar, R. Delaigle and P. Eloy, Elaboration and characterization of sulfated and unsulfated V_2O_5/TiO_2 nanotubes catalysts for chlorobenzene total oxidation, *Appl. Catal., B*, 2014, **147**, 58–64.

7 S. Chin, E. Park, M. Kim, G. N. Bae and J. Jurng, Effect of the support material (TiO_2) synthesis conditions in chemical vapor condensation on the catalytic oxidation for 1,2-dichlorobenzene over V_2O_5/TiO_2, *Powder Technol.*, 2012, **217**, 388–393.

8 Q. Lan, F. B. Li, C. X. Sun, C. S. Liu and X. Z. Li, Heterogeneous photodegradation of pentachlorophenol and iron cycling with goethite, hematite and oxalate under UVA illumination, *J. Hazard. Mater.*, 2010, **174**, 64–70.

9 S. Sanches, M. T. Barreto Crespo and V. J. Pereira, Drinking water treatment of priority pesticides using low pressure UV photolysis and advanced oxidation processes, *Water Res.*, 2010, **44**, 1809–1818.

10 M. Fukushima and K. Tatsumi, Degradation pathways of pentachlorophenol by photo-Fenton systems in the presence of iron(III), humic acid, and hydrogen peroxide, *Environ. Sci. Technol.*, 2001, **35**, 1771–1778.

11 R. Vargas and O. Núnez, The photocatalytic oxidation of dibenzothiophene (DBT), *J. Mol. Catal. A: Chem.*, 2008, **294**, 74–81.

12 K. Hanna, Ch. de Brauer, P. Germain, J. M. Chovelon and C. Ferronato, Degradation of pentachlorophenol in

cyclodextrin extraction effluent using a photocatalytic process, *Sci. Total Environ.*, 2004, **332**, 51–60.

13 C. C. Dong, J. H. Ji, Z. Yang, Y. F. Xiao, M. Y. Xing and J. L. Zhang, Research progress of photocatalysis based on highly dispersed titanium in mesoporous SiO_2, *Chin. Chem. Lett.*, 2019, **30**, 853–862.

14 M. Y. Xing, Y. Zhou, C. Y. Dong, L. J. Cai, L. X. Zeng, B. Shen, L. H. Pan, C. C. Dong, Y. Chai, J. L. Zhang and Y. D. Yin, Modulation of the Reduction Potential of TiO_{2-x} by Fluorination for Efficient and Selective CH_4 Generation from CO_2 Photoreduction, *Nano Lett.*, 2018, **18**, 3384–3390.

15 B. Wang, G. X. Zhang, X. Leng, Z. M. Sun and S. L. Zheng, Characterization and improved solar light activity of vanadium doped TiO_2/diatomite hybrid catalysts, *J. Hazard. Mater.*, 2015, **285**, 212–220.

16 S. Rehman, R. Ullah, A. M. Butt and N. D. Gohar, Strategies of making TiO_2 and ZnO visible light active, *J. Hazard. Mater.*, 2009, **170**, 560–569.

17 T. Z. Tong, J. L. Zhang, B. Z. Tian, F. Chen and D. N. He, Preparation of Fe^{3+}-doped TiO_2 catalysts by controlled hydrolysis of titanium alkoxide and study on their photocatalytic activity for methyl orange degradation, *J. Hazard. Mater.*, 2008, **155**, 572–579.

18 H. Yamashita, H. Harada, J. Misaka, M. Takeuchi, K. Ikeue and M. Anpo, Degradation of propanol diluted in water under visible light irradiation using metal ion-implanted titanium dioxide photocatalysts, *J. Photochem. Photobiol., A*, 2002, **148**, 257–261.

19 R. A. Doong, P. Y. Chang and C. H. Huang, Microstructural and photocatalytic properties of sol–gel-derived vanadium-doped mesoporous titanium dioxide nanoparticles, *J. Non-Cryst. Solids*, 2009, **355**, 2302–2308.

20 H. Li, G. L. Zhao, Z. J. Chen, G. R. Han and B. Song, Low temperature synthesis of visible light-driven vanadium doped titania photocatalyst, *J. Colloid Interface Sci.*, 2010, **344**, 247–250.

21 M. Vijayakumar, S. Kerisit, C. M. Wang, Z. M. Nie, K. M. Rosso, Z. G. Yang, G. Graff, J. Liu and J. Z. Hu, Effect of Chemical Lithium Insertion into Rutile TiO_2 Nanorods, *J. Phys. Chem. C*, 2009, **113**, 14567–14574.

22 Q. Y. Li, T. Kako and J. H. Ye, Strong adsorption and effective photocatalytic activities of one-dimensional nano-structured silver titanates, *Appl. Catal., A*, 2010, **375**, 85–91.

23 C. R. Xiong, X. Y. Deng and J. B. Li, Preparation and photodegradation activity of high aspect ratio rutile TiO_2 single crystal nanorods, *Appl. Catal., B*, 2010, **94**, 234–240.

24 K. Melghit and K. Bouziane, Room temperature ferromagnetism of iron-doped rutile TiO_2 nanorods synthesized by a low temperature method, *J. Alloys Compd.*, 2008, **453**, 102–107.

25 H. Zhu, J. Tao and X. Dong, Preparation and Photoelectrochemical Activity of Cr-Doped TiO_2 Nanorods with Nanocavities, *J. Phys. Chem. C*, 2010, **114**, 2873–2879.

26 X. Li, M. Yoneda, Y. Shimada and Y. Matsui, Effect of surfactants on the aggregation and stability of TiO_2 nanomaterial in environmental aqueous matrices, *Sci. Total Environ.*, 2017, **574**, 176–182.

27 M. J. Ren, H. Horn and F. H. Frimmel, Aggregation behavior of TiO_2 nanoparticles in municipal effluent: influence of ionic strengthen and organic compounds, *Water Res.*, 2017, **123**, 678–686.

28 H. Y. Lin and C. Y. Shih, Efficient one-pot microwave-assisted hydrothermal synthesis of M (M = Cr, Ni, Cu, Nb) and nitrogen co-doped TiO_2 for hydrogen production by photocatalytic water splitting, *J. Mol. Catal. A: Chem.*, 2016, **411**, 128–137.

29 J. F. Niu, P. Lu, M. Kang, K. F. Deng, B. H. Yao, X. J. Yu and Q. Zhang, P-doped TiO_2 with superior visible-light activity prepared by rapid microwave hydrothermal method, *Appl. Surf. Sci.*, 2014, **319**, 99–106.

30 F. T. Lia, X. J. Wang, Y. Zhao, J. X. Liu, Y. J. Hao, R. H. Liu and D. S. Zhao, Ionic-liquid-assisted synthesis of high-visible-light-activated N-B-F-tri-doped mesoporous TiO_2 via a microwave route, *Appl. Catal., B*, 2014, **144**, 442–453.

31 X. B. Li, L. L. Wang and X. H. Lu, Preparation of silver-modified TiO_2 via microwave-assisted method and its photocatalytic activity for toluene degradation, *J. Hazard. Mater.*, 2010, **177**, 639–647.

32 P. L. Zhang, S. Yin and T. Sato, Synthesis of high-activity TiO_2 photocatalyst via environmentally friendly and novel microwave assisted hydrothermal process, *Appl. Catal., B*, 2009, **89**, 118–122.

33 J. N. Hart, D. Menzies, Y. B. Cheng, G. P. Simon and L. Spiccia, A comparison of microwave and conventional heat treatments of nanocrystalline TiO_2, *Sol. Energy Mater. Sol. Cells*, 2007, **91**, 6–16.

34 P. Peng, X. D. Liu, C. S. Sun, J. M. Ma and W. J. Zheng, Facile fabrication of rutile monolayer films consisting of well crystalline nanorods by following an IL-assisted hydrothermal route, *J. Solid State Chem.*, 2009, **182**, 1003–1008.

35 T. Lavanya, M. Dutta, S. Ramaprabhu and K. Satheesh, Superior photocatalytic performance of graphene wrapped anatase/rutile mixed phase TiO_2 nanofibers synthesized by a simple and facile route, *J. Environ. Chem. Eng.*, 2017, **5**, 494–503.

36 R. Verma and S. K. Samdarshi, Correlating oxygen vacancies and phase ratio/interface with efficient photocatalytic activity in mixed phase TiO_2, *J. Alloys Compd.*, 2015, **629**, 105–112.

37 P. L. Zhang, B. Liu, S. Yin, Y. H. Wang, V. Petrykin, M. Kakihana and T. Sato, Rapid synthesis of nitrogen doped titania with mixed crystal lattice via microwave-assisted hydrothermal method, *Mater. Chem. Phys.*, 2009, **116**, 269–272.

38 X. T. Jia, W. He, X. D. Zhang, H. S. Zhao, Z. M. Li and Y. J. Feng, Microwave-assisted synthesis of anatase TiO_2 nanorods with mesopores, *Nanotechnology*, 2007, **18**, 3205–3210.

39 S. Cerneaux, X. Y. Xiong, G. P. Simon, Y. B. Cheng and L. Spiccia, Sol–gel synthesis of SiC–TiO_2 nanoparticles for microwave processing, *Nanotechnology*, 2007, **18**, 2341–2346.

40 L. Li, C. Y. Liu and Y. Liu, Study on activities of vanadium (IV/V) doped TiO_2(R) nanorods induced by UV and visible light, *Mater. Chem. Phys.*, 2009, **113**, 551–557.
41 D. Agrawal, Latest global developments in microwave materials processing, *Mater. Res. Innovations*, 2010, **14**, 3–8.
42 F. Spadavecchia, G. Cappelletti, S. Ardizzone, C. L. Bianchi, S. Cappelli, C. Oliva, P. Scardi, M. Leoni and P. Fermo, Solar photoactivity of nano-N-TiO_2 from tertiary amine: role of defects and paramagnetic species, *Appl. Catal., B*, 2010, **96**, 314–322.
43 K. Kočí, K. Matějů, L. Obalová, S. Krejčíková, Z. Lacný, D. Plachá, L. Čapekc, A. Hospodková and O. Šolcová, Effect of silver doping on the TiO_2 for photocatalytic reduction of CO_2, *Appl. Catal., B*, 2010, **96**, 239–244.
44 K. Chen, J. Y. Li, J. Li, Y. M. Zhang and W. X. Wang, Synthesis and characterization of TiO_2-montmorillonites doped with vanadium and/or carbon and their application for the photodegradation of sulphorhodamine B under UV-vis irradiation, *Colloids Surf., A*, 2010, **360**, 47–56.
45 R. Jaiswal, N. Patel, D. C. Kothari and A. Miotello, Improved visible light photocatalytic activity of TiO_2 co-doped with vanadium and nitrogen, *Appl. Catal., B*, 2012, **126**, 47–54.
46 D. P. Xu, L. J. Feng and A. L. Lei, Characterizations of lanthanum trivalent ions/TiO_2 nanopowders catalysis prepared by plasma spray, *J. Colloid Interface Sci.*, 2009, **329**, 395–403.
47 S. Yuan, Q. R. Sheng, J. L. Zhang, H. Yamashita and D. N. He, Synthesis of thermally stable mesoporous TiO_2 and investigation of its photocatalytic activity, *Microporous Mesoporous Mater.*, 2008, **110**, 501–507.
48 D. Z. Lu, B. Zhao, P. F. Fang, S. B. Zhai, D. L. Li and Z. Q. Chen, Facile one-pot fabrication and high photocatalytic performance of vanadium doped TiO_2-based nanosheets for visible-light-driven degradation of RhB or Cr(VI), *Appl. Surf. Sci.*, 2015, **359**, 435–448.
49 X. F. Chang, J. Huang, Q. Y. Tan, M. Wang, G. B. Ji, S. B. Deng and G. Yu, Photocatalytic degradation of PCP-Na over BiOI nanosheets under simulated sunlight irradiation, *Catal. Commun.*, 2009, **10**, 1957–1961.